Astron. Astrophys. 338, 1057–1065 (1998)

ASTRONOMY AND ASTROPHYSICS

Ultraviolet and optical flares on Gl 866

D. Jevremović[1,5], C.J. Butler[1], S.A. Drake[2], D. O'Donoghue[3,4], and F. van Wyk[4]

[1] Armagh Observatory, College Hill, Armagh BT61 9DG, Northern Ireland (djc@star.arm.ac.uk; cjb@star.arm.ac.uk)
[2] Goddard Space Flight Center, NASA, Greenbelt, MD 20771, USA
[3] Department of Astronomy, University of Cape Town, Rondebosch 7700, South Africa
[4] South African Astronomical Observatory, P.O. Box 9, Observatory 7935, South Africa
[5] Astronomical Observatory, Volgina 7, 11070 Belgrade, Yugoslavia

Received 17 February 1998 / Accepted 2 June 1998

Abstract. We present simultaneous ultraviolet and optical observations of five flares on the very late type M dwarf Gl 866 (dM5.5e). A procedure to estimate the physical parameters of the flaring plasma has been developed using a simplified model of the flare and a comparison of observed and computed Balmer decrements. With this procedure we have determined the optical thickness, electron temperature and electron density of the flaring plasma at flare maximum for three spectroscopically observed flares. The three spectroscopically observed flares cover up to 5 percent of the stellar surface and have areas similar to solar flares.

Key words: stars: activity – binaries: spectroscopic – stars: chromospheres – stars: flare – stars: late-type

1. Introduction

Flares on late type stars are widely believed to arise from magnetic processes similar to those that drive the better known solar flares. This, canonical, view is based on the similar characteristics of their optical, ultraviolet and X-ray emission (see Butler, 1993). As observational data becomes available with a time resolution compatible with the time-scale of flare events it should eventually be possible to explore the physical parameters of the flares in greater detail and to make a more meaningful comparison between solar and stellar events. In this paper we attempt to model the behaviour of the hydrogen line emission from several flares on the late-M type dwarf star Gliese 866 in order to determine physical parameters such as the temperature, density and volume of the flaring plasmas.

Gl 866 (EZ Aqr) is a very late type (dM5.5e) nearby dwarf star (d=3.4 pc). Leinert et al.(1986) and McCarthy et al. (1987) found that Gl866 is also a double star and subsequently Leinert et al. (1990) have determined the orbital and physical parameters of the system. They find effective temperatures of 2900K and 2500-2750K, and masses of 0.22 $M_\odot$ and 0.16 $M_\odot$, for the primary and secondary, respectively. Gl 866 is a known flare star (Kunkel, 1972) and an X-ray source (Johnson, 1984).

Send offprint requests to: D. Jevremović

2. Observations

Simultaneous optical spectroscopy, optical photometry, ultraviolet spectroscopy and X-ray monitoring of Gliese 866 were scheduled for 10/11 June 1991. The optical data were obtained at the South African Astronomical Observatory (SAAO) and the ultraviolet spectroscopy with International Ultraviolet Explorer (IUE). Regrettably, X-ray observations by the Röntgen Satellite (ROSAT) were cancelled at the last moment due to problems with on-board instrumentation. The log of successful observations is shown in Table 1 and a time-line for the observations illustrated in Fig. 1.

2.1. Photometry

The photometric data were obtained with the standard single-channel photometer attached to the SAAO 0.5m telescope with Cape/Kron UBVR$_c$ and Hβ (narrow and wide) filters. Integration times were: 10s in the U and Hβ (narrow and wide), 2s in the B and 1s in the V and R filters and the comparison star was SAO 165227 (Sp.K0III, m$_v$=8.4, B-V=1.2). We have reduced the UBVR observations to the standard Cousins system using the measured extinction coefficients k$_v$=0.15, k$_b$=0.27 k$_u$=0.54 and k$_r$=0.10 and the colour equations determined in May 1991 by Kilkenny and Marang (private communication).

From the average count rates we have found the formal errors of the Gl866 photometry to be 0.03, 0.04, 0.02 and 0.01 magnitudes for U,B,V and R$_c$ respectively.

The narrow Hβ filter is assumed to measure the line flux plus a small amount of adjacent continuum, whereas the wide Hβ filter measures line flux together with a larger portion of continuum. We have reduced the Hβ photometry in the following way: firstly we have corrected the raw counts for dead-time losses, sky background and atmospheric extinction and secondly we have subtracted the continuum counts (scaled by the ratio of the FWHM of the two filters) to get true "line-only" counts, according to the formula:

$$C(H\beta) = C_N - \frac{(C_W - C_N)}{(\Delta\lambda_W - \Delta\lambda_N)} \times \Delta\lambda_N$$

Table 1. GL 866 Observing Log:1991 June 10/11

Observer	Telescope	Type of data	Time (UT)	Filters/Spectral coverage
F. van Wyk	SAAO 0.5m	Optical photometry	23:47-04:03	UBVR+Hβ(n+w)
D. O'Donaghue	SAAO 1.9m	Optical spectroscopy	23:46-04:40	3600-5400 Å
C.J. Butler	IUE Vilspa	Ultraviolet spectroscopy(SWP)	23:33-03:53	1150-2000 Å
		Ultraviolet spectroscopy(LWP)	22:17-04:46	1900-3100 Å

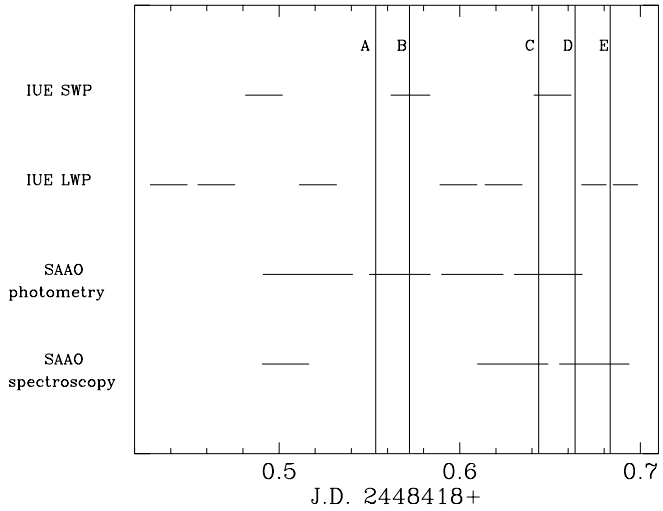

Fig. 1. The time-line for observations of Gl866 on the night 10/11 June 1991. Vertical lines show the start times of the five flares detected.

where C_N, C_W are the counts in the narrow and wide filters respectively and $\Delta\lambda_N$ and $\Delta\lambda_W$ are their FWHM.

2.2. Optical spectroscopy

Optical spectroscopy has been carried out with the 1.9m telescope at SAAO with the RGO Spectrograph. The wavelength coverage was 3400-5400 Å at a reciprocal dispersion of 100 Å/mm and a wavelength resolution of $\Delta\lambda \sim 4$ Å(FWHM). Spectra were recorded using the Intensified Reticon Photon Counting System with an exposure time of 60^s and a time resolution of 70^s. A total of 140 spectra were obtained. Each spectrum was wavelength calibrated by reference arc spectra observed approximately once per hour. The absolute flux calibration has been achieved using observations of a flux standard to correct the wavelength dependance and scaling to match fluxes in the photometric B band. We estimated this calibration to be accurate to $\pm 20\%$ over the range 3800Å to 5000Å. At shorter wavelengths, fluxes could be less accurate.

2.3. UV spectroscopy

Ultraviolet spectroscopy was obtained with the International Ultraviolet Explorer (IUE) satellite described in Boggess et al. (1978). The log of the IUE observations is shown in Table 2. The usable spectral range extends from 1150 to 2000 Å in the short wavelength region (SWP camera) and 1900 to 3100 Å in the long wavelength region (LWP camera).

All IUE spectra were reduced from the photometrically corrected images using the STARLINK package IUEDR.

In order to improve the time resolution, two LWP spectra were exposed per image by placing the star at opposite ends of the large aperture. With the Starlink IUEDR package we were subsequently able to separate the two spectra into a and b components (see Table 2)

3. Results

3.1. Photometry

The light curves in the UBVR filters are shown in Fig. 2. There are four flares detectable in U, three of which are also seen in B. Two of the flares, marked A and D, have very short spiky light curves, suggestive of compact events. The third flare (C) has a double peak in U with an initial, short, impulsive phase followed by a second rise and a relatively prolonged decay.

For comparison with other physical parameters of flares it is necessary to convert the UBVR$_c$ magnitudes into absolute fluxes. This was achieved by reference to tables by Bessell (1979) for a star with M_V=0. The total time-integrated fluxes, minus the quiescent levels, for those flares observed photometrically, are given in Table 3. We have assumed a distance of 3.4 parsec for Gliese 866 and that the observed fluxes are emitted over 4π steradians.

From Table 3 one can see that the flare energies radiated in each photometric band are similar, but the contrast between a flare and the quiescent level is much higher in the U band. This contrast can be easily seen if one divides the energy radiated during each flare by the quiescent level to obtain the so called "equivalent duration" of the flare (eg. Gershberg 1972, van den Oord et al. 1996). For Flare C the equivalent duration is about 600s in U, 150s seconds in B, 45s in V and only 25 seconds in R.

3.2. Measurements of Hβ

The light curves in Hβ, obtained from photometry and spectroscopy, together with changes in the continuum near Hβ, are shown in Fig. 3. Where there is overlap between the photometric and spectroscopic coverage we note the significantly improved signal to noise ratio obtainable with the 1.9m telescope spectroscopy compared to the 0.5m telescope photometry. Using the

Table 2. IUE observations of Gl 866 on the night 10/11 June 1991. Units for line fluxes are $10^{-14} erg\ cm^{-2} s^{-1}$.

Spectrum	Start UT	Exp. s	FeII 2590	FeII 2625	AlII 2669	FeII 2750	MgII 2800	Cont. 2850-3100
LWP20566a	22:17	1800	4	6	2	9	21	63
LWP20566b	22:55	1800	3	6	3	7	23	53
LWP20567a	00:16	1800	3	4	0	5	20	78
LWP20567b	00:54	1800	3	4	3	5	22	60
LWP20568a	02:08	1800	2	0	0	9	23	65
LWP20568b	02:44	1800	1	0	0	8	18	33
LWP20569a	04:01	1200	4	7	4	0	32	35
LWP20569b	04:26	1200	0	0	7	5	45	120
SWP41815	23:33	1800						
SWP41816	01:29	1800						
SWP41817	03:23	1800						

Table 3. Continuum energy radiated during quiescence and during flares on Gliese 866 together with the start time and duration of each flare. Note that the units for quiescent flux are $erg \times s^{-1}$

Flare	UT	Dur. s	U (erg)	B (erg)	V (erg)	R (erg)	3600-3700 (erg)	4120-4320 (erg)	4400-4800 (erg)
Quies.($\times s^{-1}$)	-	-	1.9×10^{27}	1.6×10^{28}	4.8×10^{28}	2.3×10^{29}	6.8×10^{25}	4.8×10^{26}	6.9×10^{27}
A	1:17	1320	8.1×10^{29}	8.4×10^{29}	2.1×10^{30}	4.9×10^{30}	-	-	-
B	1:44	1250	8.7×10^{29}	1.6×10^{30}	2.4×10^{30}	3.3×10^{30}	-	-	-
C	3:27	1830	1.1×10^{30}	2.5×10^{30}	2.1×10^{30}	6.2×10^{30}	1.2×10^{29}	8.6×10^{28}	1.0×10^{30}
D	3:56	1720	$3.2\times10^{29*}$	$1.5\times10^{30*}$	$5.2\times10^{29*}$	$2.2\times10^{30*}$	8.1×10^{28}	6.0×10^{28}	9.8×10^{29}
E	4:24	1090*	-	-	-	-	$2.6\times10^{29*}$	$2.9\times10^{29*}$	$2.7\times10^{30*}$

* - incomplete measurement

calibrated spectrophotometric Hβ flux from the 1.9m we were subsequently able to calibrate the 0.5m Hβ photometry. The middle panel in Fig. 3, shows the calibrated flux in Hβ from the 0.5m observations.

3.3. Optical spectroscopy

Firstly, we have co-added the 75 quiescent spectra of Gliese 866 to form a mean quiescent spectrum. This is shown, together with the spectrum of flare D taken at 04:23 UT, in Fig. 4. The Balmer lines from Hβ to H8 and the CaII H and K lines are visible in the quiescent spectrum. In the flare spectrum the Balmer lines up to H13, HeI($\lambda\lambda$4461,4026 Å) and CaI (λ4226Å) lines are in emission and there is a substantially enhanced ultraviolet continuum.

In order to obtain the time profiles of fluxes in the hydrogen, calcium and helium lines we subtracted the mean quiescent spectrum from each flare spectrum and integrated the fluxes in carefully chosen windows which include the emission lines. Windows either side of the emission lines are also binned to provide continuum levels. Time profiles of the integrated Balmer line fluxes, corrected for continuum, are shown in Fig. 5 and for the CaI/II and helium lines in Fig. 6. There are three flares visible, two of which (C and D) are also detected in the U band. Our medium resolution spectroscopy cannot resolve the CaII H and Hϵ line, but from Fig. 6 it is clear that the blend is dominated by the behaviour of Hϵ. We note the comparatively slow response of the CaII K line compared to the Balmer lines.

We integrated the fluxes in time and by scaling them to the intrinsic stellar values got the total energies irradiated during each flare. Those energies are listed in Table 4 for all lines. Energies irradiated in the three continuum regions: 3600-3700Å, 4130-4350Å (with exclusion region of the CaI line) and 4400-4800Å, are listed in Table 3. From the integrated fluxes in the Hγ line we conclude that the flares detected on Gliese 866 are typical for dMe stars and at the upper end of the range of observed solar flare Hγ fluxes (see eg. Table 3 in Butler et al. (1988) and Fig. 2 in Butler (1993)).

3.4. Ultraviolet spectroscopy

During the eight hour IUE shift, three SWP spectra and four double exposure LWP spectra were obtained. The three SWP spectra were under-exposed and show no discernible features other than geo-coronal Lyman α. Unfortunately, in the second exposure, during which a small flare was detected photometrically, a cosmic ray hit has destroyed any information there may have been on the intensity of the CIV doublet at 1550 Å. Excluding Hα, this line would normally be the strongest in the SWP range for dMe stars in flare.

Table 4. Times of flare maxima and total energies irradiated in Balmer, Calcium, Helium and Magnesium lines. Units are 10^{28}erg

Flare	Time	H10	H09	H08	CaIIK	CaIIH+Hϵ	HeI	Hδ	CaI	Hγ	HeI	Hβ	Hβ_{ph}	MgII
A	1:17	-	-	-	-	-	-	-	-	-	-	-	6.8	-
B	1:44	-	-	-	-	-	-	-	-	-	-	-	4.5	-
C	3:27	4.7	5.3	8.3	9.0	18.9	0.8	13.2	0.9	17.6	1.2	27.0	33.4	-
D	3:56	1.4	2.7	6.2	5.4	11.2	1.1	8.7	0.3	11.9	1.0	20.1	12.2*	17.4
E	4:24	4.3	6.9	9.8	12.2	22.3	.05	17.7	0.06	25.9	1.1	38.4	-	40.3

* - incomplete measurement

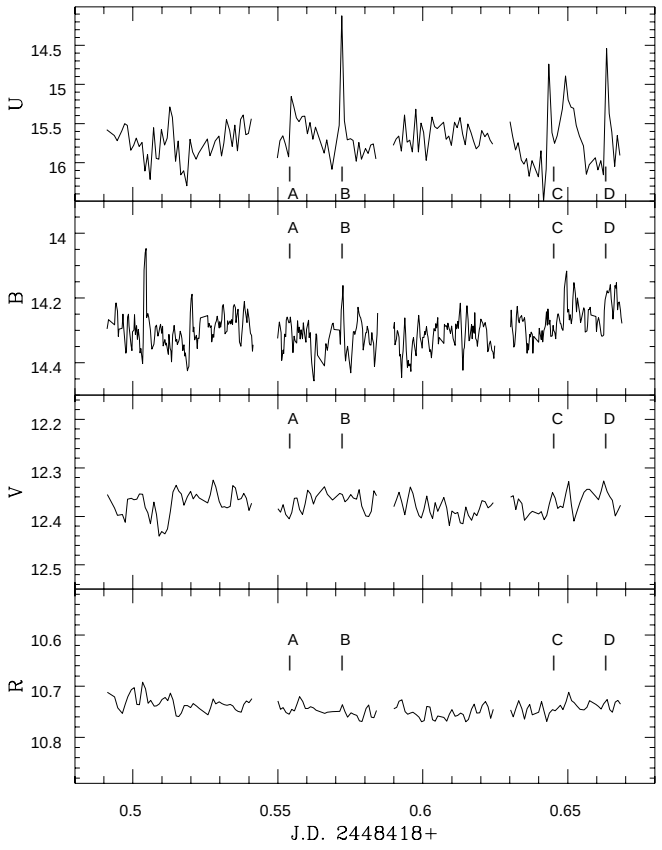

Fig. 2. Light curves in U, B, V and R_c with the start of the detected flares A-D indicated

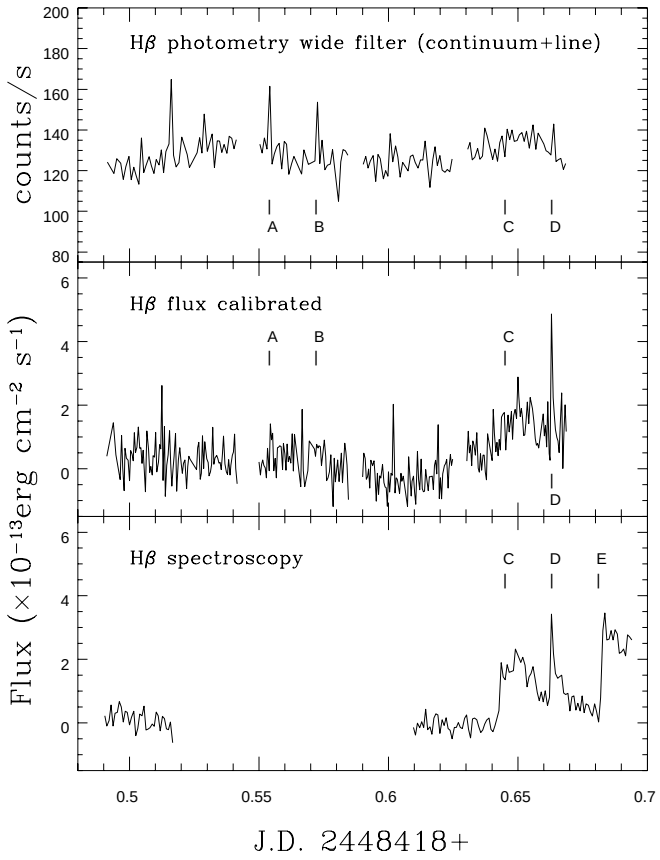

Fig. 3. The photometry in the Hβ line obtained with 0.5m telescope. For comparison, we plot in the lower panel, the light curve obtained from spectroscopy.

The four double LWP exposures, which were interleaved with the SWP exposures, had a detectable signal in the middle of their range. After the separation and calibration of the two components, a and b on each image, we examined the resultant eight low dispersion near UV spectra for presence of the MgII (2800Å) and AlII (2669Å) resonance lines and also for the numerous FeII (2590Å, 2620Å, 2735Åand 2775Å) lines. The integrated fluxes for these lines, corrected for continuum, together with continuum flux between 2850 and 3100 Å are listed in Table 2. Within the accuracy of measurement, the fluxes in Table 2 are constant, except for the last two spectra during which the MgII lines are significantly enhanced. As one can see from Fig. 1 these two spectra were recorded shortly after flares D and E had reached their maximum in the optical emission lines. As it is expected that the MgII emission during a flare would be delayed even more than the CaII emission (see Gurzadyan, 1984) we feel reasonably sure that the enhanced fluxes in the last two LWP spectra result from flares D and E respectively. Probably as a result of this delay in MgII emission, Flare B, which occurred shortly before the end of exposure LWP 20567b, does not appear to have been detected by IUE. In Fig 7 we show the quiescent and flare LWP spectra over the range 2500-3200Å, and in Table 4 we give the energy irradiated in the MgII doublet.

The continuum flux, between 2850 and 3100 Å, is significantly enhanced only in the last recorded spectrum, namely

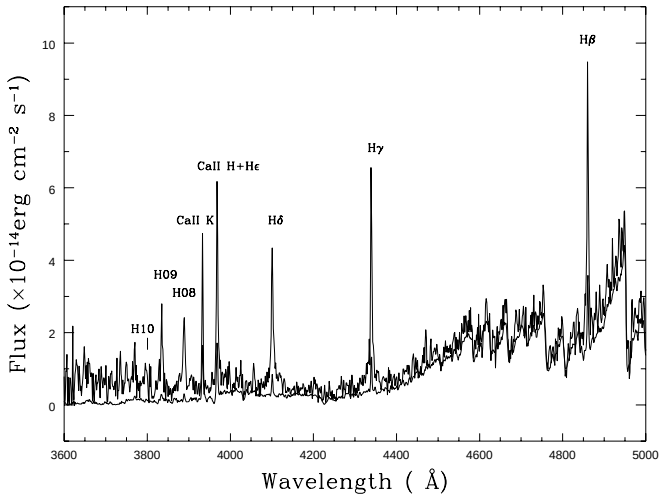

Fig. 4. The mean quiescent spectrum and the spectrum recorded at 04:23 UT during flare D. Balmer lines up to H13 and CaII K and H(superposed with Hϵ) are clearly visible.

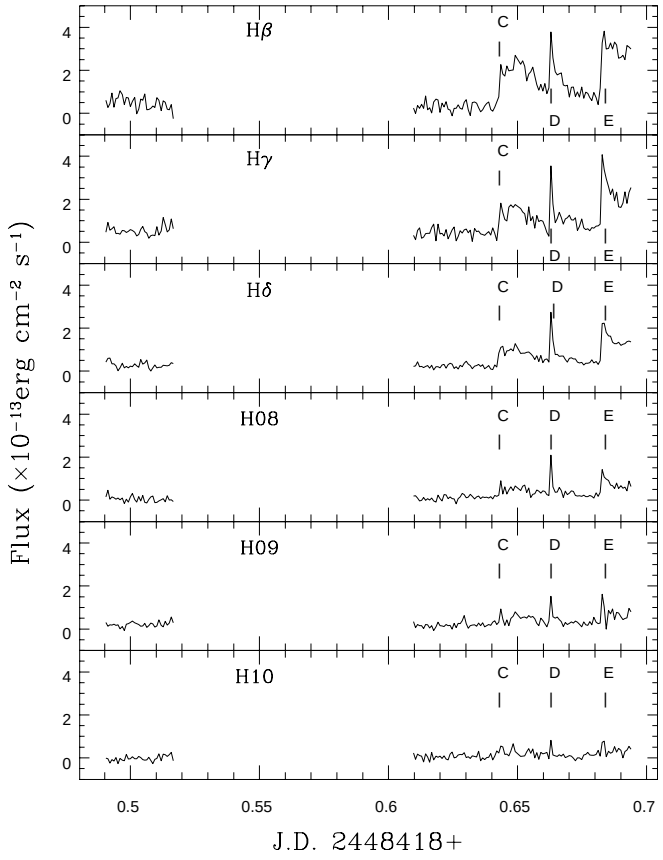

Fig. 5. Time profiles of the fluxes in the Balmer lines.

LWP20569b. This we attribute to flare E, the most powerful of the five flares recorded.

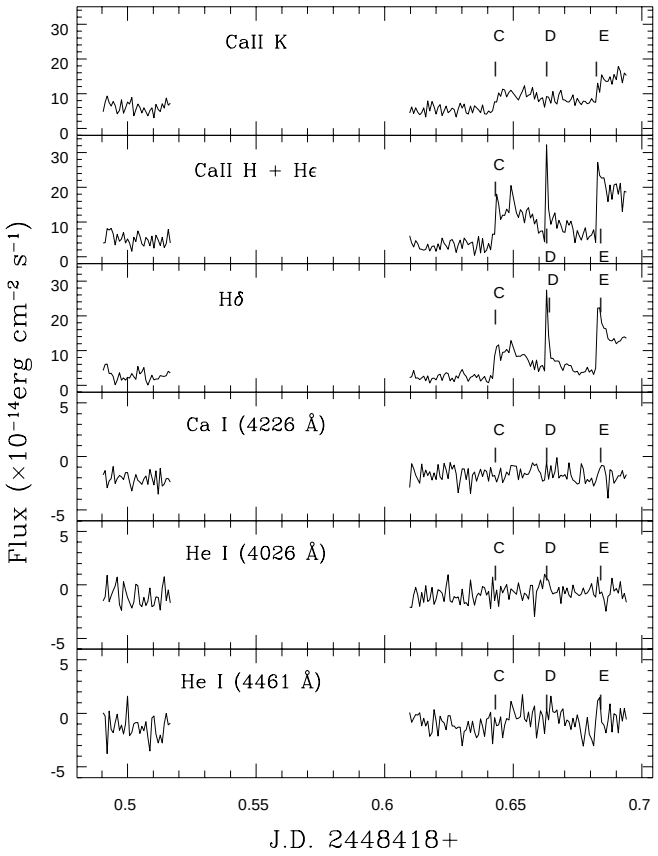

Fig. 6. Time profiles of the fluxes in the calcium and helium lines together with the Hδ line. Note that the behaviour of the CaII H+ Hϵ blend is dominated by Hϵ

4. Determination of plasma properties

Several different mechanisms have been considered to model the transport of energy from the stellar corona, where the magnetic reconnection is believed to take place, to lower layers during stellar flares; namely: heat conduction, X-ray irradiation (e.g. Hawley & Fisher 1992), a beam of energetic electrons (e.g. Houdebine 1992) and a beam of protons (van der Oord, 1988). Recently, Katsova et al.(1997) has explored a gas-dynamic simulation for an impulsively heated flare on a dM star. They found the source of the continuum radiation to be a dense condensation which propagates down towards the photosphere. In all studies significant changes in the chromospheric and photospheric structure are necessary to reproduce the observed spectral characteristics.

It is widely accepted that the source of white light during flares must lie deep in the dense photospheric layers where the number of emitting particles is sufficient to produce a significant rise in continuum flux. The line emission, on the other hand, is believed to originate higher in the stellar atmosphere; in the chromosphere. Balmer decrements (ratios between Hn and Hγ, henceforth referred to as BD) are relatively good indicators of the properties of the flaring plasma (Katsova 1990). Very steep Balmer decrements indicate a plasma with N_e between 10^8 and 10^{12} cm^{-3} and large optical depths in Hα and very shallow

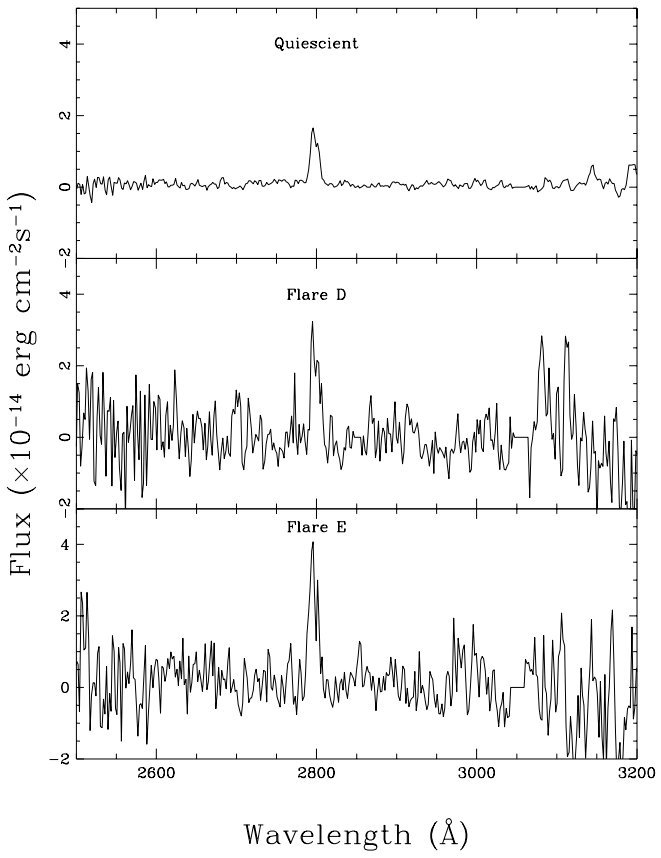

Fig. 7. IUE Long wavelength spectra

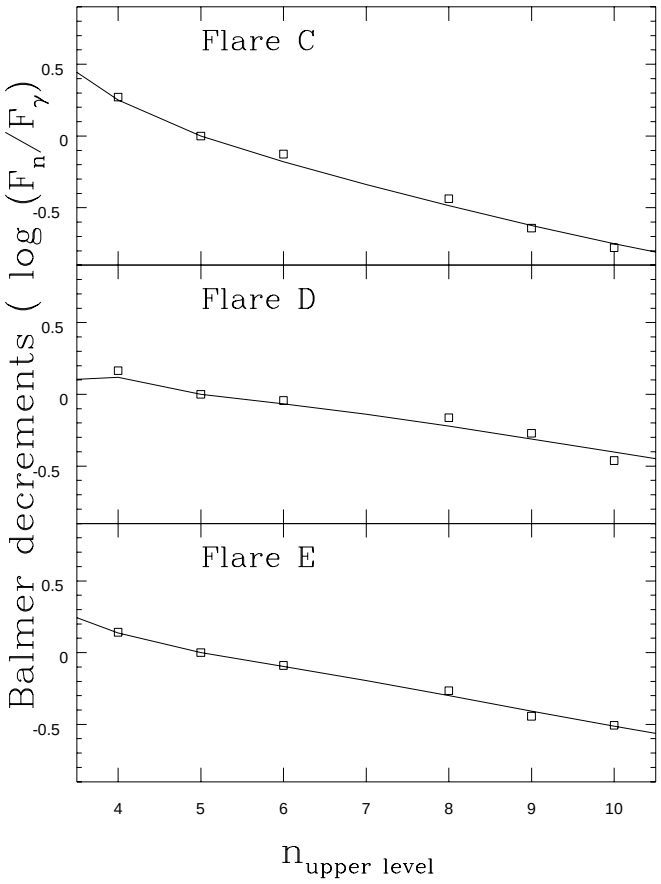

Fig. 8. The observed Balmer decrements at flare maxima and the optimum computed fits from varying τ(Lyα), T_e and N_e of the emitting plasma for flares C, D and E

Balmer decrements indicate electron densities larger than 10^{13} cm^{-3} (Drake 1980).

We developed a procedure to fit the BD based on the solution of the radiative transfer equation using the escape probability method of Drake (1980) and Drake & Ulrich (1980). This method considers that the escape probability for a slab of optical thickness is averaged over direction assuming a uniform distribution of emitters, complete redistribution of frequencies and the line profile represented by a Doppler core and power law wings of slope -5/2.

We adopted a simplified picture of the flaring plasma as a slab of hydrogen with an underlying thermal source of radiation which causes photoionization. In this picture we assume that the Balmer lines are formed in the upper chromosphere. In the case of the typical flare plasma, with a temperature of 15000K and an electron density of 10^{14}cm^{-3}, the underlying thermal source with a temperature of 8000K induces five orders of magnitude more photoionization events than collisional processes due to thermal motion of the electrons. Therefore, the underlying source dominates the ionization balance of the flare plasma.

We tried to find the best possible solution for the BD in four-parameter space, where the parameters are: electron temperature, electron density, optical depth in the Lyman α line and the temperature of the underlying source.

Our procedure minimizes the difference between the observed and calculated BD using a multi-directional direct search algorithm (eg. Torczon 1991, Torczon 1992). Details of this algorithm are given in the Appendix.

The results of fits for the flare maxima for three spectroscopically observed flares are shown in Fig. 8 and the best fit parameters are shown in Table 5. From the figure we can see that the fits achieved in approximately two to three hundred iterations are very good.

In order to check our results, we calculated the differences between the theoretical and observed Balmer decrements for the following grid of values: the electron density between 10^{10} and 10^{17} cm^{-3}, electron temperatures between 4000 and 40000 K, and $\tau(Ly\alpha)$ between 10^3 (optically thin case) and 10^6 (optically thick case) using the same computational procedure for radiative transfer, but keeping the temperature of the underlying source constant(4000K). The results of this test calculation for the maximum of Flare D are shown in Fig. 9. This illustrates the full complexity of the problem of estimating values for these parameters in multi-dimensional space.

The next problem one faces when fitting multi-parameter functions is to estimate the confidence domains of the parameters. We have used the $\Delta_3 = \frac{1}{\sigma^2}S$ function of

Cherepashchuk(1993) where S represents the sum of the squares of the differences between the fitted and observed functions. Δ_3 behaves as χ^2_k where k is the number of degree of freedom (number of points fitted - in our case five). We can define the confidence domains for estimated parameters as a subset of parameters for which Δ_3 is less than $\chi^2_{k,\gamma}$. Using a simple recording procedure inside the function evaluation routine, we were able to estimate lower limits for the confidence domains with a confidence level of γ=90% for the derived parameters (Table 5). It is noticeable that increasing the confidence level leads to confidence domains which tend to cover a very large volume of parametric space.

From the best fit solutions for the Balmer decrements we calculated the effective thicknesses of the slabs of hydrogen plasma for the three flares. Subsequently we were able to determine the surface area of the emitting plasma from the calculated emission measure and the measured fluxes in H_β. The results are also shown in the Table 5.

From Table 5 we can see that the three flares display different characteristics. Flare C has a relatively high optical depth in the Lyα line but a relatively low temperature and electron density. This is as expected from the steep Balmer decrement of flare C (see Fig. 8 and Drake, 1980). The optimum fits for flares D and E constrain the temperatures and optical depth in Lyα to similar values, however the more shallow Balmer decrement of flare D requires a higher electron density than for flare C. We note the different behaviour of the model predictions for the undefined region $n_{upperlevel} < 4$, (flux ratio between Hα and Hγ). Simultaneous observations of Hα would be required to constrain the models in this region.

For flares C and E we found large areas of emitting plasma. Taking into account that the radius of the hotter component is about 0.2 $R_\odot$ (Leinert et al. 1990) one can calculate that flares C, D and E cover 5, 0.1 and 1 percent of the stellar surface area, respectively. Thus flares C and E have sizes comparable with those of the largest solar flares; i.e. a few times $10^{19} cm^2$ (eg. Tandberg-Hanssen & Emslie, 1988)

From the emissivity curve of the Hγ line, Houdebine et al.(1991) estimated the flare maximum temperature to be about 17000 K. The effective temperature of the emitting plasma we determined for flare C is lower than the temperature Houdebine et al. (1991) assigned to flare maxima. From the light curve for this flare one can see that this is a typical example of an impulsive flare with a prolonged gradual phase and therefore their discussion may not apply. Another reason for the discrepancy may be that, in their approach, Houdebine et al. use only one line, whereas our procedure uses six lines. The temperatures determined for flares D and E are more consistent with the value given by Houdebine et al. (1991).

The effective thickness, electron density and relatively small area for flare D are consistent with the gas-dynamic simulations of an impulsively heated flare given by Katsova et al. (1997). In the case of flare E, the effective thickness of the emitting plasma is about a thousand kilometres. This value is influenced by the fact that the ionization balance around 20000K is changing very rapidly and, as the electron temperature rises, we need a thicker slab of plasma to have the same optical depth. Nagai & Emslie (1984) studied the hydrodynamic response of the Solar atmosphere to impulsive heating and in their Case A (multiple energy releases of very short duration) found a layer of about five thousand kilometers thick with a temperature of about 30000K. An alternative explanation could be that, in the case of flare E, material is ejected into the corona by heating. Katsova et al.(1997) obtained typical evaporation velocities of the order of tens to two hundred kilometers per second. Unfortunately, the time and spectral resolution presently available does not allow us to resolve such evaporation. From the volume of emitting plasma, the computed electron density and, by assigning a typical velocity of 100 km/s, (and bearing in mind that Drake and Ulrich's solution of radiative transfer is not fully applicable for such a high velocity), one can estimate the kinetic energy of potential evaporation to be $\sim 10^{30}$ erg. This value is comparable to the total energy irradiated in the Balmer lines.

5. Conclusions

Five flares were detected either photometrically or spectroscopically on Gliese 866. The energies radiated by those flares are comparable with the strongest solar ones but are of medium strength compared to flares on other dMe stars. The high flare activity rate is probably connected with the binary nature of this system.

A powerful procedure is developed for the determination of the properties of the plasma from Balmer decrements using a direct search method in multi-dimensional space. This procedure can be used in other multi-parameter problems.

The physical properties we have determined are consistent with the standard picture of stellar flares, and we found potential evidence of coronal mass ejection for one flare.

Further observations with a higher time and spectral resolution are desirable.

Acknowledgements. Research at Armagh Observatory is grant-aided by the Department for Education, N. Ireland. The authors thank G. Djurašević for valuable discussions and E.R.Houdebine and B. van der Oord for useful comments on an earlier draft of this paper. The IUE observation included in this paper were obtained by the ESA Satellite Tracking Station at Vilspa, Spain.

Appendix

In this appendix we briefly describe the multi-directional search algorithm we used to derive our plasma flare parameters

An iteration of the basic multi-directional search algorithm for minimizing some function $f(\mathbf{v})$ (in our case a sum of the squares of the differences between observed and calculated Balmer decrements) begins with a simplex S in $\mathcal{R}^n$, with vertices $\mathbf{v}_0, \mathbf{v}_1, ..., \mathbf{v}_n$. In Fig. A1 we show the two-dimensional case. The vertex $\mathbf{v_0}$ is defined as the vertex with the lowest value of $f(\mathbf{v})$ for which $f(\mathbf{v}_0) \leq f(\mathbf{v_j}), j = 1, ..., n$. The first step is to reflect $\mathbf{v_1}, ..., \mathbf{v_n}$ through the vertex $\mathbf{v_0}$ to obtain the reflected vertices $\mathbf{r_j}$. If a reflected vertex gives a lower value of $f(\mathbf{v})$, we designate that reflection step is successful. The algorithm

Table 5. The results of the fit of Balmer decrements using the direct search method. We derive the following parameters for the flare maxima: $\tau(L\alpha)$, electron temperature, electron density and temperature of the underlying source together with the calculated emission measure, the effective thickness D and the surface area A for three spectroscopically observed flares. Confidence domains are also given for the fitted parameters for a confidence level of 90%.

Flare	$log\tau(Ly\alpha)$	log N_e	T_e	T_{us}	EM(Hβ) ($ergcm^{-3}s^{-1}$)	D (km)	A (cm^2)	Δ_3
C	6.74	12.5	8020	3960	2.1	2.2	6.5e19	4.4
conf.dom.	6.5-6.8	12.3-12.8	7900-8200	3900-4100				
D	4.31	14.9	16110	3780	10900	0.52	7.9e17	6.3
conf.dom.	4.2-4.7	14.8-15.1	15900-17400	3600-3800				
E	4.24	12.5	20630	7180	0.21	1140	1.5e19	1.9
conf.dom.	4.1-4.4	12.2-12.7	19900-21400	6700-7600				

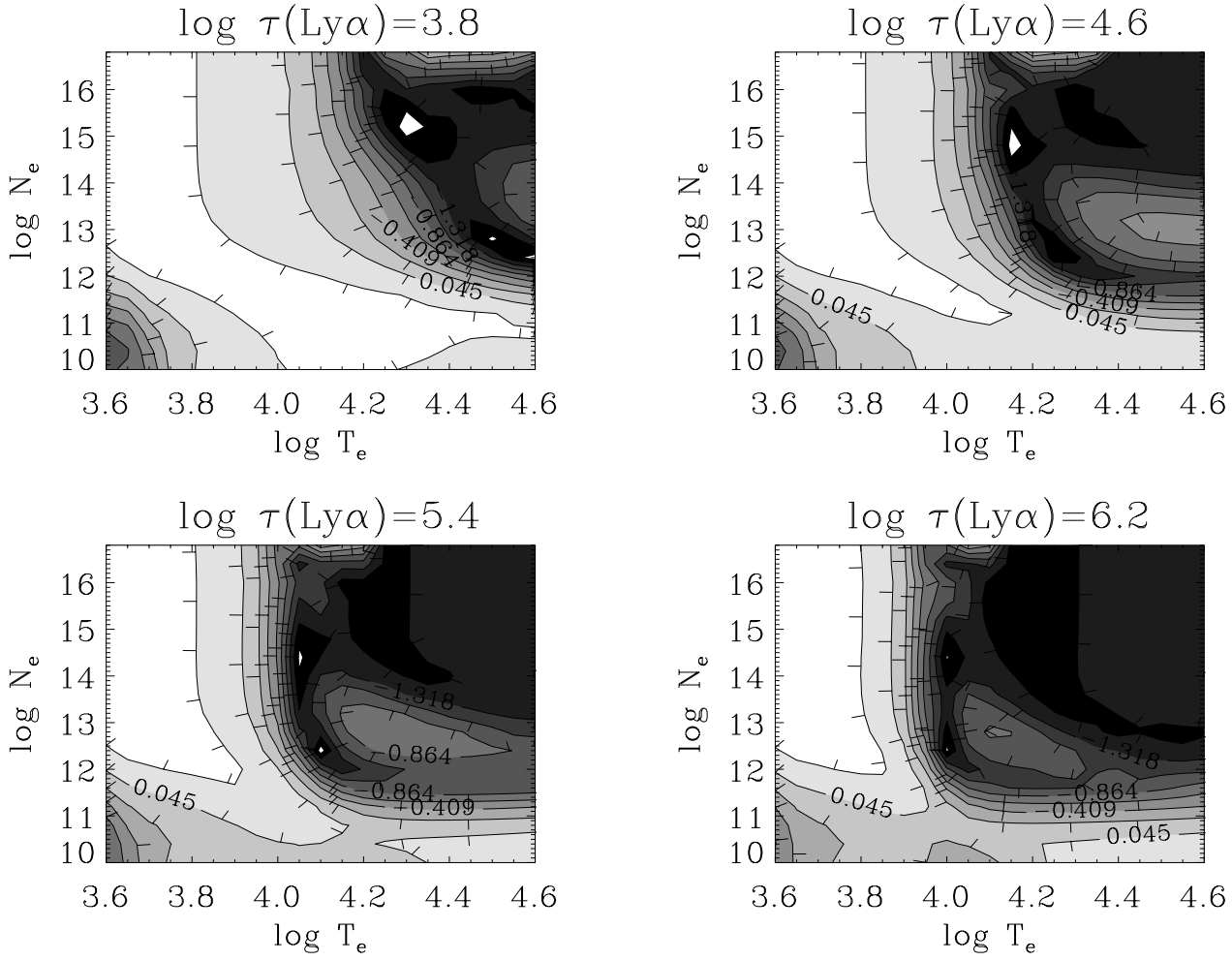

Fig. 9. Contour plots of the logarithm of the sum of the squares of the differences between the observed and calculated Balmer decrements for different τ(Lyα) for Flare D and a temperature of the underlying source of 4000 K. The small white areas inside the darkest part of the plot indicate the closest fit between the observed and calculated Balmer Decrements

then moves to an expansion step which consists of expanding each reflected edge $(\mathbf{r_j} - \mathbf{v_0})$ to twice its length to give a new vertex $\mathbf{e_j}$(see Fig. A1). In an iteration of this basic algorithm, the expansion step would be tried only if the reflection step was successful, and it would be accepted only if the expansion vertex was better than all reflection vertices. Thus if we take the expansion step, the new simplex S_+ is either the expansion simplex $< \mathbf{v_0}, \mathbf{e_j} >$ or the reflection simplex $< \mathbf{v_0}, \mathbf{r_j} >$. In the case where the reflection step was unsuccessful, i.e. no reflection vertex has a better function value than $f(\mathbf{v_0})$ we take S_+ (the new

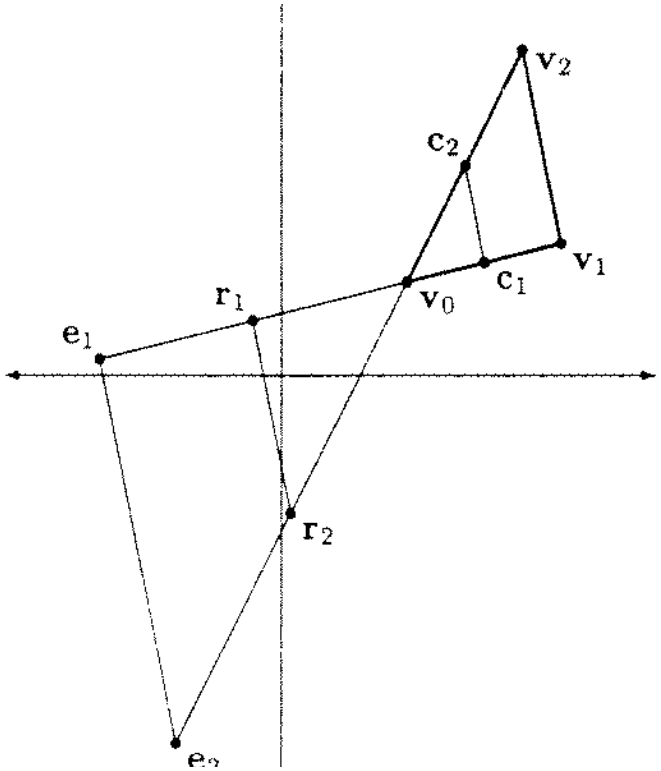

Fig. A1. Possible steps in multidirectional search method in the two-dimensional case.

simplex) to be the contraction simplex formed by replacing each vertex of the worst n-face in the original simplex by the point midway from it to the best vertex $< \mathbf{v_0}, \mathbf{c_j} >$ (see Fig. A1). To complete one iteration of the basic algorithm we take $\mathbf{v_0^+}$ to be the best vertex of S_+. We repeat this basic algorithm until either the exit condition is satisfied (difference between "calculated" and "observed" function value is less than some given value) or the maximum number of iterations is reached.

The principal difference between this algorithm and the classical and the more popular simplex search algorithm of Nelder and Mead (1965) lies in the fact that Nelder and Mead's algorithm does not search in each of n linearly independent search directions at every iteration. As Torczon (1991) proved, her multidirectional algorithm converges for functions which are continuously differentiable over some subset of the domain. The proof can be extended to treat most non-smooth cases of interest; the argument only breaks down only at points where the derivative exists, but is not continuous.

References

Bessell M.S., 1979, PASP 91, 589
Boggess A., Carr F.A., Evans D.C. et al., 1978, Nature 275, 372
Butler C.J., 1993, A&A 272, 507
Butler C.J., Rodono M., Foing B.H. 1988, A&A 206, L1
Cherepashchuk A.M., 1993, Astron. Repo. 37(6), 585
Drake S.A., 1980, PhD thesis, UCLA
Drake S.A., Ulrich R.K., 1980, ApJS 42, 351
Gershberg R.E., 1972, ApSS 19, 75
Gurzadyan G.A. 1984, ApSS 106, 1
Hawley S.L., Fisher G.H., 1992, ApJS 78, 565
Houdebine E.R., 1992, Irish Astron. J. 20, 248
Houdebine E. R., Butler C. J., Panagi P. M., Rodono M., Foing B. H., 1991, A&AS 87, 33
Johnson H.M. 1984, in *Activity in red-dwarf stars*, P.B. Byrne and M. Rodono, eds, Reidel, Dordrecht, p.109
Katsova M.M., 1990, Sov. Astron. 34, 614
Katsova M.M., Boiko A. Ya., Livshits M. A.,1997, A&A 321, 549
Kunkel W.E. 1972, Inform. Bull. Var. Stars no.748
Leinert Ch., Jahrei H., Haas M, 1986, A&A 164, L29
Leinert Ch., Haas M., Allard F. et al., 1990, A&A 236, 399
McCarthy Jr.,Cobb M.L., Probst R.G., 1987, AJ 93, 1535
Nagai F., Emslie A.G. 1984, ApJ 279, 896
Nelder J.A., Mead R, 1965, Comput. J. 7, 308
van den Oord G.H.J., 1988, A&A 207, 101
van den Oord G.H.J., Doyle J.G., Rodono M. et al., 1996, A&A 310, 908
Tandberg-Hanssen E., Emslie G., 1988, *The physics of solar flares*, Cambridge, p.7
Torczon V., 1991, SIAM J.Optimization, Vol.1, No.1, 123
Torczon V., 1992, Tech. Report 92-9, Dept. of Mathematical Sciences, Rice University, Houston